MRS Communications (2018), *8*, 1311–1320

doi:10.1557/mrc.2018.158

MRS Communications

Research Letter

Fabrication, microstructure, and enhanced thermionic electron emission properties of vertically aligned nitrogen-doped nanocrystalline diamond nanorods

Kamatchi Jothiramalingam Sankaran, Institute for Materials Research (IMO), Hasselt University, 3590 Diepenbeek, Belgium; IMOMEC, IMEC vzw, 3590 Diepenbeek, Belgium
Sujit Deshmukh, Department of Physics, School of Natural Sciences, Shiv Nadar University, NH-91, Tehsil Dadri, Gautam Buddha Nagar, Uttar Pradesh 201314, India
Svetlana Korneychuk, Electron Microscopy for Materials Science (EMAT), University of Antwerp, 2020 Antwerp, Belgium
Chien-Jui Yeh, Department of Engineering and System Science, National Tsing Hua University, Hsinchu, Taiwan, Republic of China
Joseph Palathinkal Thomas, WATLab and Department of Chemistry, University of Waterloo, Waterloo, N2L3G1 Ontario, Canada
Sien Drijkoningen, Paulius Pobedinskas, and **Marlies K. Van Bael,** Institute for Materials Research (IMO), Hasselt University, 3590 Diepenbeek, Belgium; IMOMEC, IMEC vzw, 3590 Diepenbeek, Belgium
Johan Verbeeck, Electron Microscopy for Materials Science (EMAT), University of Antwerp, 2020 Antwerp, Belgium
Keh-Chyang Leou, Department of Engineering and System Science, National Tsing Hua University, Hsinchu, Taiwan, Republic of China
Kam-Tong Leung, WATLab and Department of Chemistry, University of Waterloo, Waterloo, N2L3G1 Ontario, Canada
Susanta Sinha Roy, Department of Physics, School of Natural Sciences, Shiv Nadar University, NH-91, Tehsil Dadri, Gautam Buddha Nagar, Uttar Pradesh 201314, India
I-Nan Lin, Department of Physics, Tamkang University, 251 Tamsui, Taiwan
Ken Haenen, Institute for Materials Research (IMO), Hasselt University, 3590 Diepenbeek, Belgium; IMOMEC, IMEC vzw, 3590 Diepenbeek, Belgium

Address all correspondence to Kamatchi Jothiramalingam Sankaran and Ken Haenen at **sankaran.kamatchi@uhasselt.be** and **ken.haenen@uhasselt.be**

(Received 21 June 2018; accepted 26 July 2018)

Abstract

Vertically aligned nitrogen-doped nanocrystalline diamond nanorods are fabricated from nitrogen-doped nanocrystalline diamond films using reactive ion etching in oxygen plasma. These nanorods show enhanced thermionic electron emission (TEE) characteristics, viz., a high current density of 12.0 mA/cm^2 and a work function value of 4.5 eV with an applied voltage of 3 V at 923 K. The enhanced TEE characteristics of these nanorods are ascribed to the induction of nanographitic phases at the grain boundaries and the field penetration effect through the local field enhancement from nanorods owing to a high aspect ratio and an excellent field enhancement factor.

Introduction

The conversion of thermal waste energy into electrical energy makes thermionic electron emission (TEE) a promising renewable energy source. Contrary to the field electron emission behavior, in which the emitted electrons are extracted from the materials due to band bending induced by an external applied field, TEE implies the heat-induced emission of charge carriers over a surface-potential barrier typically into vacuum space.[1–4] The TEE is usually modeled by Richardson–Dushman (R–D) theory: $J_{TEE} = A_R \times T^2 \exp\left[-(\varphi - 3.79E^{1/2})/k_B T\right]$, where J_{TEE} is the TEE current density in units of A/cm^2, A_R is the Richardson constant (in units of A/cm^2 K^2), T is the temperature (in units of K), φ is the work function of the emitter (in units of eV), and k_B is the Boltzmann constant ($k_B = 1.38 \times 10^{-23}$ J/K).[4] Among these TEE parameters, the φ and A_R are the two most important materials' characteristics, which influence the J_{TEE}-value. Tables SI and SII of the Supplementary information show, respectively, the φ and the A_R values of the refractory metals, nano-carbon materials, and doped diamond, respectively, which are the commonly used cathode materials.

Apparently, high-temperature operability is a prime important characteristic needed for the materials to be served as cathode for a TEE device. In the early development of the TEE devices, refractory metals such as tungsten, molybdenum, and rhenium are the materials of choice due to their high-temperature stability. However, these refractory metals possess large work function (4–5 eV) (Table SI of the Supplementary information) and thereafter can attain large J_{TEE} value only at a temperature higher than 1000 °C that limits the potential of these materials for practical device applications. Coating low work function metals such as cesium on refractory metal lowered effectively the work function of 1.36 eV of the emitting surface (Table SI of the Supplementary information). However, the cesium coating is not stable, as it is vaporized easily at high temperature, rendering the devices not so reliable. Coating a nitrogen-doped nanocrystalline diamond films

(N-DFs) on the refractory metals can also effectively lower the work function of the tungsten (or molybdenum) materials but the Richardson constant is markedly reduced [$(A_R)_{Cs/W}$ = 0.69–1.69 A/cm^2 K^2] (Table SI of the Supplementary information) that, in turn, reduced significantly the J_{TEE}-values attainable for the TEE devices. Similarly, nanocarbon materials [such as carbon nanotubes (CNTs), carbon nanoflakes and graphene] also possess high-temperature stability with large Richardson constant [$(A_R)_{CNTs}$ = 228 A/cm^2 K^2] (Table SI of the Supplementary information), which has great potential for inducing large J_{TEE}-value, but the large φ value of 4.54 eV of the materials increases appreciably the operation temperature necessary for the TEE devices.

Diamond materials are another category of wide band gap materials, which can survive high-temperature operation and have great potential for serving as cathode for TEE devices. Moreover, the φ value of the diamond materials can be lowered effectively via the incorporation of *n*-type donors, such as phosphorus, sulfur, and nitrogen (Table SII of the Supplementary information). However, TEE measurements of these donor-doped diamond materials reveal that the A_R values of diamond materials vary inconsistently, implying that the electron transport to the surface of the diamond materials is a major issue that needs further improvement. While the lowering on the work function due to donor doping has been well studied, how to enlarge the Richardson constant of the diamond materials remains unclear.

In this context, vertically aligned nitrogen-doped nanocrystalline diamond nanorods (N-DNRs) are fabricated from N-DFs by O_2 plasma-based reactive ion etching (RIE) process for enhancing the TEE properties. The N-DNRs display a work function of φ = 4.5 eV and a large Richardson constant of A_R = 18.0 A/cm^2 K^2, which lead to a high TEE current density of 12.0 mA/cm^2 with an applied voltage of 3 V at 923 K. The enhanced TEE properties of N-DNRs are ascribed to the induction of abundant nanographitic phases at the grain boundaries and the field penetration effect through the local field enhancement from nanorods owing to a high aspect ratio and an excellent field enhancement factor.

Methods

Fabrication of vertically aligned DNRs

The fabrication process of vertically aligned nanorods started with the growth of N-DFs on Si substrates. First, the (100)-oriented mirror polished *n*-type silicon (Si) substrates (1 cm × 1 cm) were cleaned with standard RCA-1 and RCA-2 procedures.[5] The cleaned Si substrates were then seeded with a water-based state-of-the-art colloidal suspension of 5 nm nanodiamond (ND) particles by spin coating.[6] Second, two types of DFs of 500 nm thick were grown on the seeded Si substrates in an ASTeX 6500 series microwave plasma-enhanced chemical vapor deposition (MWPECVD) system. To grow undoped-nanocrystalline diamond films (U-DFs), a gas mixture of CH_4 and H_2 with flow rates of 3 and 297 sccm (CH_4/H_2 = 1/99), respectively, was excited by 3000 W microwave power and at a total pressure of 30 Torr. The substrates were heated by bombardment of the plasma species, and the substrate temperature during the growth of U-DFs was around 650 °C measured using a single-color optical pyrometer, assuming an optical emission coefficient of 0.3. For the growth of N-DFs, a gas mixture of CH_4, H_2, and N_2 with flow rates of 18, 267, and 15 sccm ($CH_4/H_2/N_2$ = 6/89/5), respectively, was excited by 3000 W microwave power, and the total pressure in the chamber was retained at 30 Torr. The substrate temperature during the growth of N-DFs was assessed to be around 540 °C.

To fabricate the nanorods from the U-DFs and N-DFs, the pristine DFs were immersed in the water-based colloidal suspension of ND particles and sonicated for 10 min to adhere these nanoparticles onto the film surface [Fig. 1(a)]. The process for making ND particles suspension was reported elsewhere.[6] The number density and uniformity of these adhered ND particles depend upon the suspension characteristics and sonication time.[7] After drying, the films coated with ND particles were put into the RIE system for the fabrication of vertically aligned undoped-diamond nanorods (U-DNRs) and N-DNRs. The ND particles adhered on the surface of the film act as a hard mask for the etching process. RIE of DFs was performed using O_2 plasma (50 sccm) in a home-built DC-plasma system with a power of 150 W [Fig. 1(b)].[8] The etching time was varied from 5 to 25 min and the gas pressure was kept at 2.8 mbar. The morphology of the nanorods mainly depends on the size and etching rate of ND particles, whereas the density of the nanorods could be controlled by varying the etching condition, i.e., O_2 flow rate and DC power.

Morphologic and structural characterization

The morphology of the diamond materials was characterized using scanning electron microscopy (SEM; a FEI Quanta 200 FEG microscope). The cross-sectional-view microstructure of the N-DNRs was analyzed using an FEI Titan "cubed" microscope operated at 300 kV for annular dark-field-scanning transmission electron microscopy (ADF-STEM) with the convergence semi-angle α used was 22 mrad and collection semi-angles of the ADF detector laying in the range from 26 to 60 mrad. Spatially resolved STEM-electron energy loss spectroscopy (EELS) mapping was carried out making use of Gatan Enfinium EELS spectrometer integrated in the Titan microscope with a collection semi-angle β = 36 mrad.[9]

TEE measurements

TEE measurements were conducted in an ultra-high-vacuum system with a base pressure of 10^{-10} Torr, which contains a radiatively heated stage with a thermocoax cable (Philips Electronics) that can reach temperatures up to 1000 K. The heater temperature is controlled by a Eurotherm PID device, which monitors the read-out from a type *K* thermocouple. A circular sample (films or nanorods on Si substrates) of 2 cm in diameter was placed on the heated sample stage as emitter. The samples were exposed to a hydrogen plasma (300 sccm, 2500 W, 20 Torr, 5 min) in the MWPECVD system for H_2-termination before being transferred into the vacuum chamber. A water-cooled polished molybdenum disc

https://doi.org/10.1557/mrc.2018.158

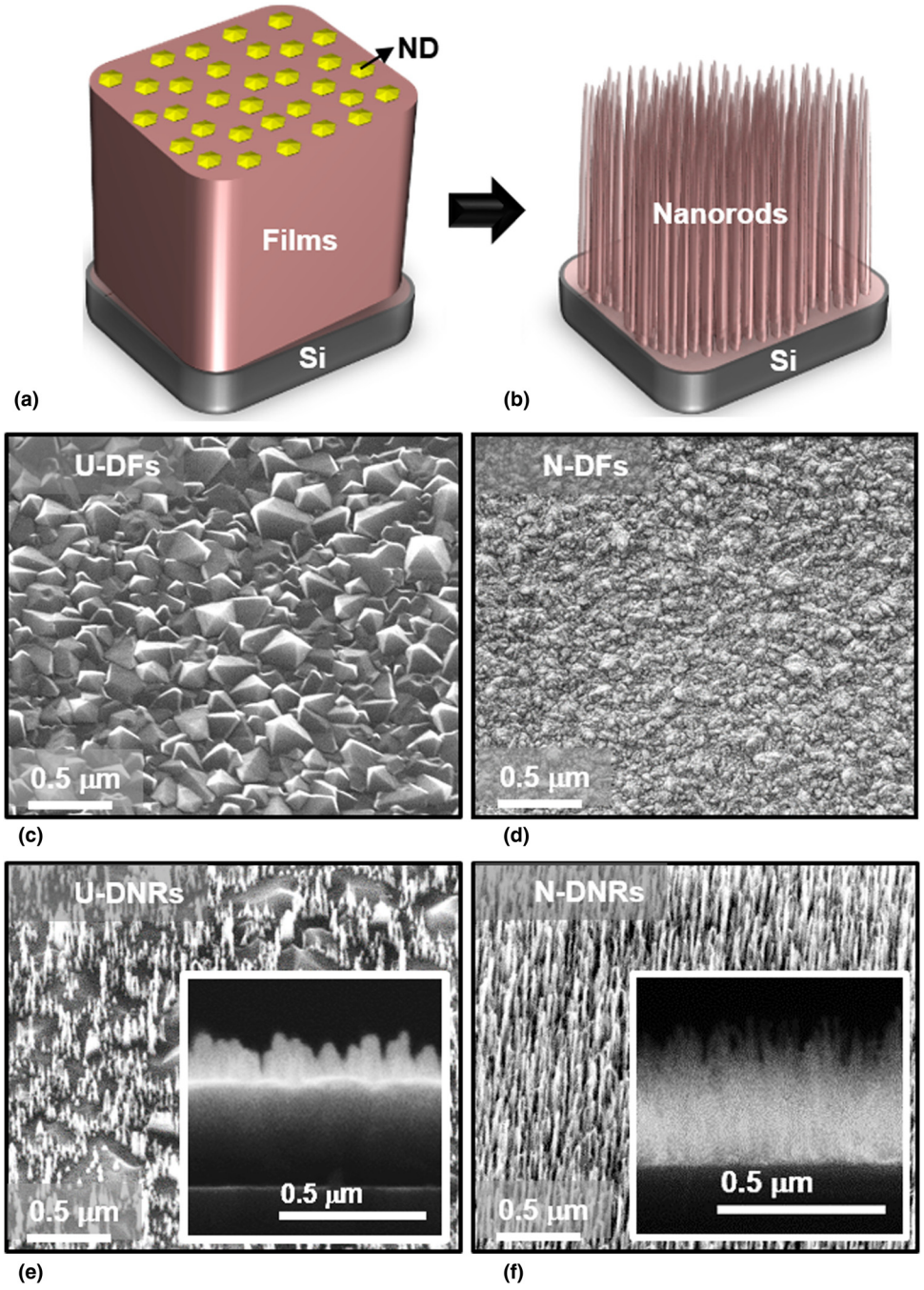

Figure 1. Schematics representation of the fabrication process of DNRs: (a) masking of the DFs with ND particles and (b) O_2 plasma-based reactive ion etching for forming DNRs. Plan-view SEM micrographs of (c) U-DFs and (d) N-DFs. (e) Tilt-view SEM micrograph of U-DNRs, along with the cross-sectional SEM micrograph as inset. (f) Tilt-view SEM micrograph of N-DNRs along with the cross-sectional SEM micrograph of N-DNRs as inset.

(2.0 cm in diameter) was used as a collector. The collector and emitter were separated by an alumina spacer of about 150 μm thick. TEE current versus applied voltage characteristics were acquired by a Keithley 2400 source-measurement unit. Typically, several measurement cycles between 300 and 973 K at various applied voltages were performed to create a stable emitter surface and to evaluate the emission current as a function of temperature and applied voltages. The application of voltages to the substrate is to overcome the space-charge effects.

Results

Figures 1(e) and 1(f) display, respectively, the tilt-view SEM images of U-DNRs and N-DNRs fabricated from U-DFs and

https://doi.org/10.1557/mrc.2018.158

N-DFs, whereas Figs 1(c) and 1(d) of the corresponding figures show the plan-view SEM images of DFs. The plan-view SEM micrographs of U-DFs [Fig. 1(c)] indicates that these films contain faceted diamond grains of sizes around ~0.4 μm, whereas the TEM micrograph in Fig. S1 of the Supplementary information reveals that the U-DFs contain very sharp grain boundaries of negligible thickness. A drastic change in surface morphology from micrometer-sized grains to nano-sized diamond grains were observed when nitrogen is incorporated into CH_4/H_2 plasma during growth process. The plan-view SEM image shown in Fig. 1(d) demonstrates that the N-DFs have a nano-sized equi-axed granular structure of size ~50 nm with a very smooth surface. The TEM characteristics of N-DFs illustrated in Fig. S2 of the Supplementary information reveals that the N-DFs contain the nano-sized grains of diamond with the abundant amorphous carbon (*a*-C) grain boundaries. These U-DFs and N-DFs were selected as the samples for the fabrication of DNRs by the O_2 plasma-based RIE process.

The fabrication of nanostructures from DFs is a very difficult task because these materials are extremely hard and chemically inert. After lots of experimentations, we finally succeeded in fabricating DNRs from DFs by using ND particles as a mask in a RIE process (in O_2 plasma). The tilt-view SEM images of U-DFs etched at different durations of 5–25 min (Fig. 2) reveal that the etching rate of U-DFs is also very slow, which is comparable with that of ND particles, such that the ND particles cannot act as the etching mask for preferentially etching of the unmasked region of U-DFs. The U-DNRs prepared via the RIE of U-DFs sparsely distributed on the samples [Fig. 1(e)]. The U-DNRs were about 90 nm in height and 100 nm in diameter [inset of Fig. 1(e)]. In contrast, Fig. 3 shows tilt-view SEM images of N-DFs after different etching durations (5–25 min), revealing that the RIE etched the DFs in a markedly larger rate than that on the ND particles. The ND particles protected very well the masked regions of N-DFs and the unmasked regions were etched gradually in a controlled manner. The morphology of N-DNRs was optimized at an etching duration of 20 min [Fig. 1(f)]. The N-DNRs were formed with very high distribution densities. These nanorods were approximately 300 nm in height and about 50 nm in diameter [inset of Fig. 1(f)]. Increasing the etching time to 25 min consumed most of ND particles such that the etching of nanorods was initiated and the nanorods become sparser than those etched for 20 min etched samples [Fig. 3(e)]. These results reveal the importance of the microstructure of the pristine DFs in the fabrication of diamond nanostructures. The etching of U-DFs is extremely difficult, since these films contain sharp grain boundaries. In contrast, the N-DFs contain large proportion of relative thick grain boundaries containing *a*-C, which facilitate the etching of DFs.

Based on these observations, a mechanism is proposed for the formation of DNRs from DFs. The N-DFs contain ND grains separated by the grain boundaries (see Fig. S2 of the Supplementary information). A large proportion of *a*-C phases exist in the grain boundaries, which is more susceptible to O_2 plasma etching than the diamond grains. At the early stage of the etching process, ND particles sitting on top of the films mask the N-DFs from being ion bombardment etched. The chemical etching of oxygen ions starts from the grain boundaries of non-masked region of the N-DFs. Because of the ease of etching the *a*-C located at the boundaries of N-DF grains, an etching path for shaping the nanorods is created, resulting in vertically aligned nanorods.[10,11] The etching process was stopped once the masking ND particles were also etched away by the O_2 plasma so as to prevent the plasma damage on the formed nanorods. The optimum etching time was determined by trial and error process. Such a technique is similar to Yang et al.'s process,[12] which utilized ND particles as a mask in a RIE process for fabricating the DNRs from ultrananocrystalline DFs. In case of U-DFs, the diamond grains are larger and there is essentially no grain boundary phase that hinders the formation of DNRs. It occurred frequently that the masked ND particles were etched away by the O_2 plasma before initiating the formation of nanorods in U-DFs. Therefore, the fabricated U-NDRs are not as densely populated and distributed less uniformly compared with N-DNRs made from N-DFs [see Figs. 1(e) and 1(f)].

Figure 4 shows the thermionic emission behavior for these diamond materials. The schematic representation of a TEE measurement is shown in the inset of Fig. 4(a). Figure 4(a) shows the J_{TEE} versus applied voltage characteristics at 773 K for DFs and DNRs. At 0 V, no electron emission is observed and after 2 V of applied voltage, the J_{TEE} starts increasing with applied voltage and tends to saturate at 15 V. In this temperature range, the electron emission from the opposite anode metal can be ignored and the emission current can be assumed to originate from the thermionic emission of the diamond cathode. The saturated J_{TEE} of the N-DNRs is approximately 35 mA/cm^2 at the applied voltage of 15 V [curve IV of Fig. 4(a)], which is significantly larger than the J_{TEE} for the N-DFs [$(J_{TEE})_{N\text{-}DF}$ = 10 mA/cm^2, curve III of Fig. 4(a)]. It is to be noted that, the J_{TEE} value attained for N-DNRs is higher than that of stacked phosphorus and nitrogen-doped DFs (18 mA/cm^2)[13] and barium strontium oxide-coated CNTs (15 mA/cm^2),[14] which are the two best TEE characteristics reported in the literature. In contrast, U-DFs and U-DNRs show lower saturated J_{TEE} values of 1.85 mA/cm^2 [curve I of Fig. 4(a)] and 2.94 mA/cm^2 [curve II of Fig. 4(a)] at the applied voltage of 15 V, respectively. The J_{TEE} versus applied voltage characteristics at different measuring temperatures (figure not shown) show similar trend with those shown in Fig. 4(a), viz., the J_{TEE} increases with applied voltage and saturates at around an applied voltage of 15 V.

Moreover, the J_{TEE} values for these samples at applied voltage of 3 V were plotted against the measuring temperature in Fig. 4(b), indicating that the TEE process for these materials starts at a temperature as low as 670 K and increases monotonically with temperature. The J_{TEE} obtained at the temperature of 923 K is 12.0 mA/cm^2 [curve IV of Fig. 4(b)] and 5.2 mA/cm^2 [curve III of Fig. 4(b)] for the N-DNRs and N-DFs, respectively.

https://doi.org/10.1557/mrc.2018.158

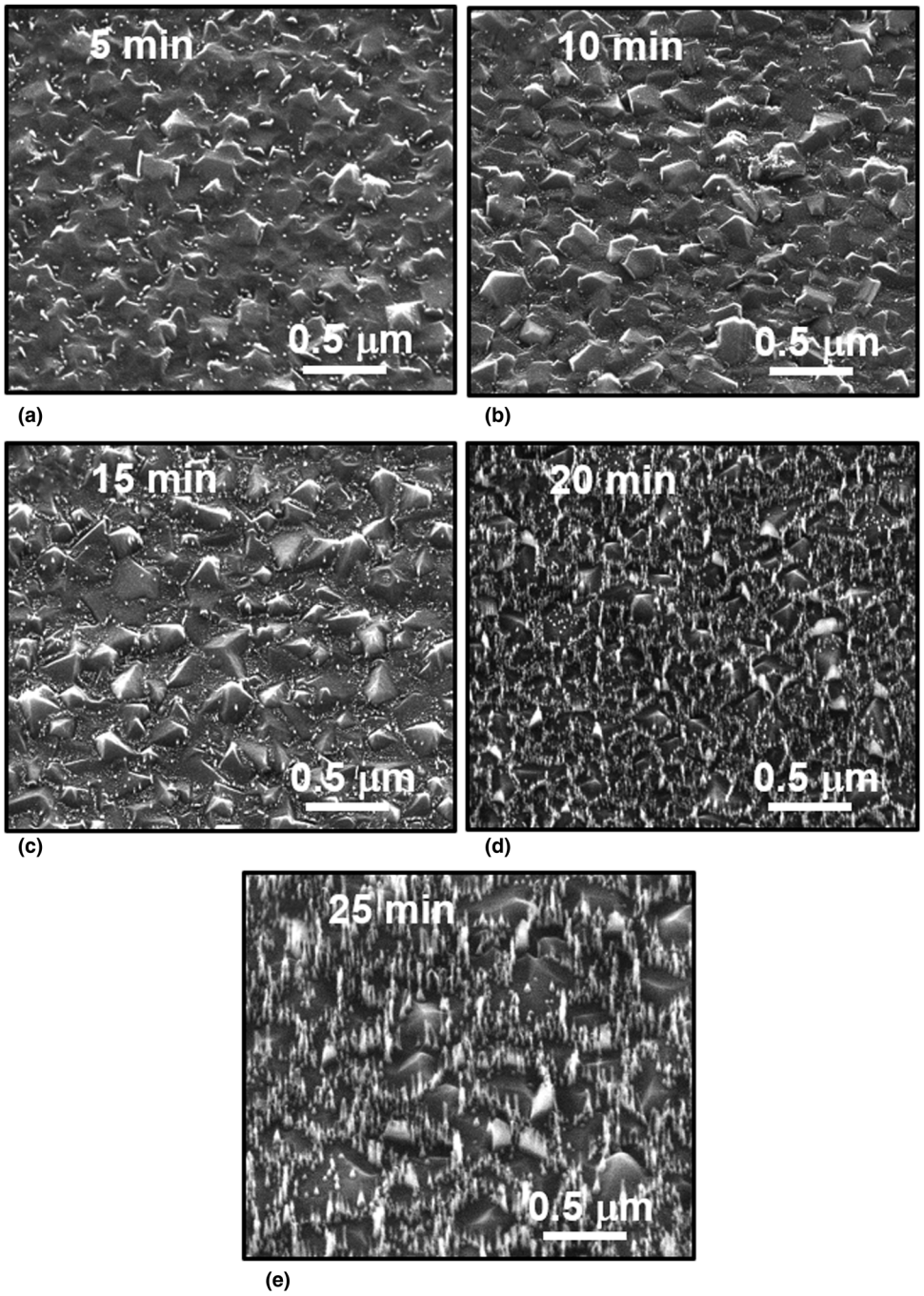

Figure 2. SEM images of the U-DF surface after RIE etching for different etching times of (a) 5 min, (b) 10 min, (c) 15 min, (d) 20 min, and (e) 25 min.

But U-DFs and U-DNRs exhibit markedly lower J_{TEE}-values of 0.5 mA/cm^2 [curve I of Fig. 4(b)] and 1.01 mA/cm^2 [curve II of Fig. 4(b)] at the temperature of 923 K. These J_{TEE} versus T curves were fitted with the R–D equation and the φ, and the A_R values of these diamond samples were estimated (summarized in Table I). The N-DNRs possess the φ value of 4.5 eV with Richardson constant of $(A_R)_{N\text{-}DNRs} = 18.0$ A/cm^2 K^2, whereas the N-DFs show a similar φ-value of 4.8 eV with a smaller Richardson constant of $(A_R)_{N\text{-}DF} = 3.8$ A/cm^2 K^2. Moreover, both U-DFs and U-DNRs own the same φ-value of around 5.0 eV, respectively, and Richardson constant of $A_R = 0.05$–0.07 A/cm^2 K^2, which are smaller as compared with those of N-DF and N-DNRs. This reveals that the RIE etching process insignificantly alters the φ-value but markedly increases the Richardson constant of N-DF series materials. It does not significantly alter these TEE parameters of the

https://doi.org/10.1557/mrc.2018.158

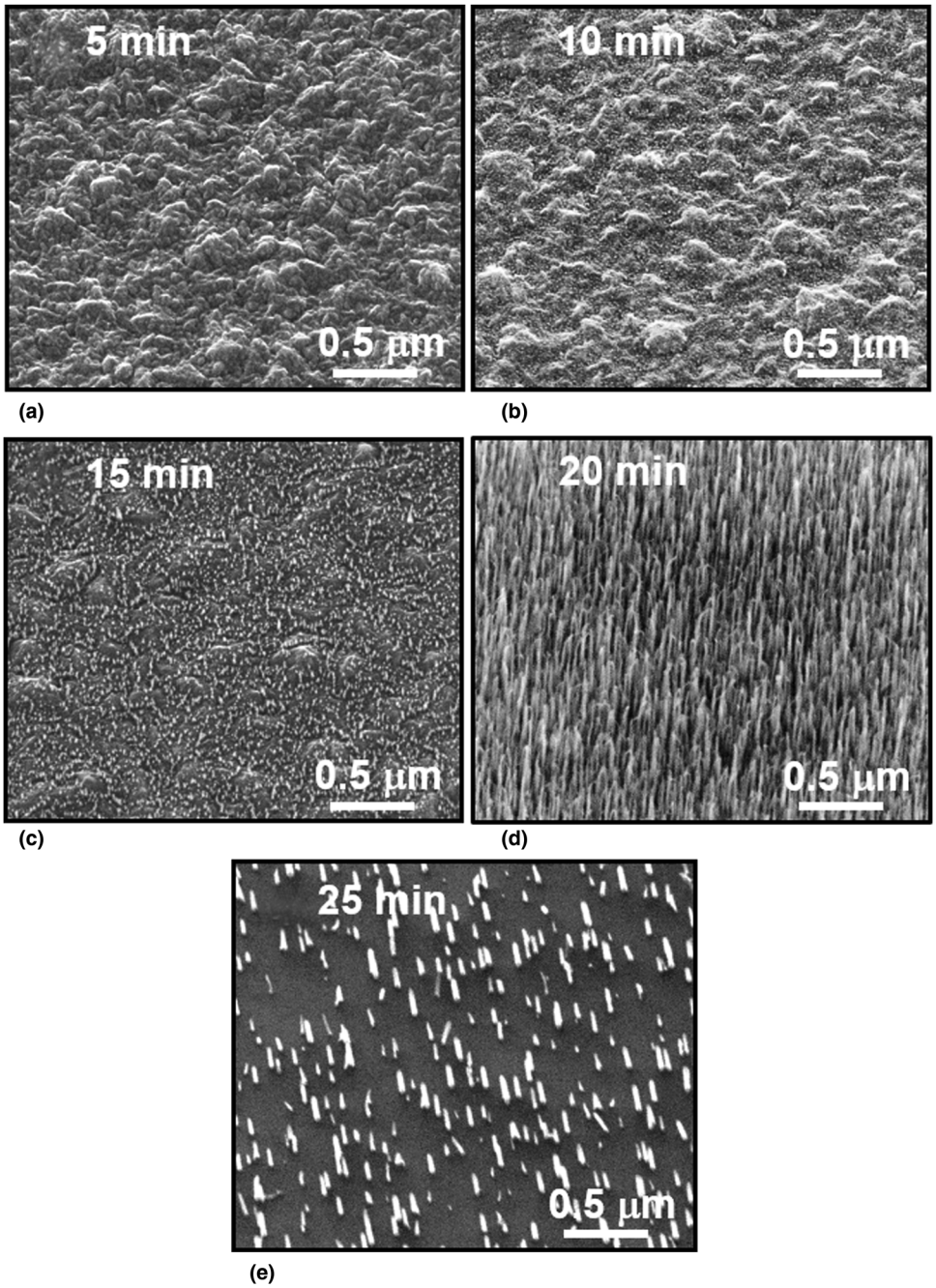

Figure 3. SEM images of the N-DF surface after RIE etching for different etching times of (a) 5 min, (b) 10 min, (c) 15 min, (d) 20 min, and (e) 25 min.

U-DF series materials. That is, only when the DFs possess good conductivity, the RIE nanostructuring process can increase the Richardson constant value of the materials. The TEE parameters listed in Table I reveal that the main factor, which leads to larger TEE current density for N-DNRs due to RIE process, is mainly owing to the increase in the value of Richardson constant. The value of work function is less significantly affected due to the nanostructuring process. Generally a proper doping is required to lower the φ-value of the diamond materials. Furthermore, to verify the accuracy of the work function value estimated from TEE measurements, Kelvin probe force microscopy (KPFM) measurements (Fig. S3 of the Supplementary information) were utilized to locally estimate the work function value of the N-DNRs. The estimated work function value for N-DNRs from KPFM was ~4.65 eV, which is close to the work function value (4.5 eV) of N-DNRs calculated using R–D equation. Furthermore, the stability of the TEE from N-DNRs was evaluated by

https://doi.org/10.1557/mrc.2018.158

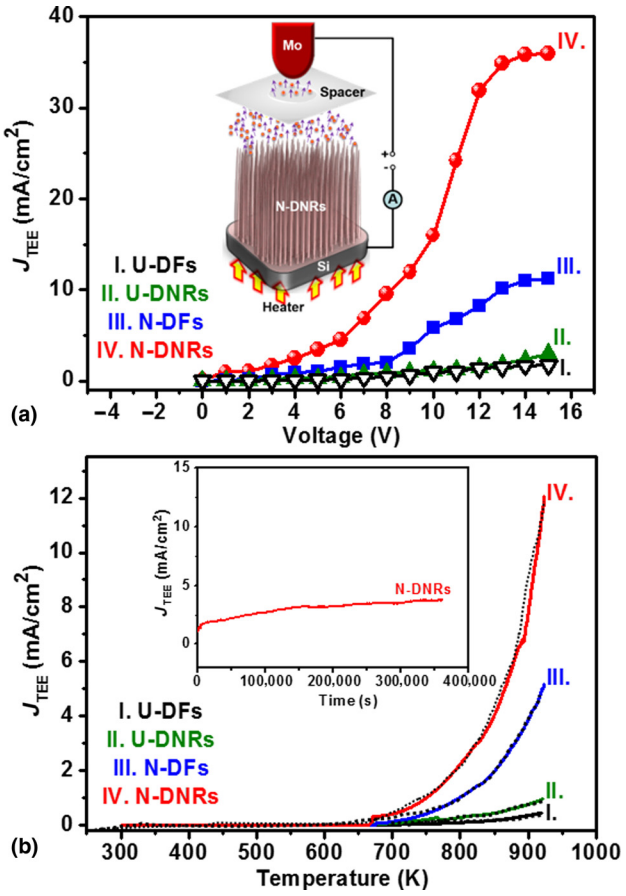

Figure 4. (a) Thermionic electron emission current density (J_{TEE}) as a function of voltage at 773 K and (b) the J_{TEE} versus temperature curves attained at an applied voltage of 3 V, fitted by the Richardson–Dushman equation, for (I) U-DFs, (II) U-DNRs, (III) N-DFs, and (IV) N-DNRs. The inset in "(a)" shows a TEE measurement setup, whereas the inset in "(b)" shows the life-time measurements, i.e., the J_{TEE} versus time curves, of N-DNRs, where the life-time measurements were carried out with a constant temperature of 773 K at an applied voltage of 3 V.

monitoring the current over a long period of time with a constant temperature of 773 K at an applied voltage of 3 V. The inset of Fig. 4(b) reveals that the J_{TEE} of 1.25 mA/cm^2 is upheld for a period over 360,000 s (6000 min) without the sign of degradation, showing high life-time stability in TEE behavior for N-DNRs.

The results described above indicate that N-DNRs possess enhanced TEE behavior (the larger J_{TEE} value) compared with the other samples examined in this study. However, understanding the microstructure of N-DNRs is required in order to clarify the key factor(s) for improving the TEE properties of N-DNRs. The detailed microstructures of N-DNRs were characterized by cross-sectional ADF-STEM. Figure 5(a) shows the nanowire of cone-shaped geometry, i.e., with diameter ranging from ~30 nm at the tip, ~60 nm at the middle, and ~80 nm at the bottom. The inset in Fig. 5(a) shows the corresponding selective area electron diffraction (SAED) pattern, which

Table I. Thermionic electron emission of U-DFs and N-DFs and their nanorods (U-DNRs and N-DNRs) at 3 V and 923 K.

Materials	Thermionic electron emission at 3 V and 923 K		
	φ (eV)	Richardson constant (A/cm^2 K^2)	J_{TEE} (mA/cm^2)
U-DFs	5.0	0.05	0.5
U-DNRs	5.0	0.07	1.01
N-DFs	4.8	3.8	5.2
N-DNRs	4.5	18.0	12.0

J_{TEE}: the TEE current density evaluated at the designated applied voltage and temperature.

φ: the TEE-based work function deduced from Richardson–Dushman model.

A_R: the Richardson constant deduced from Richardson–Dushman model.

contains sharp diffraction rings corresponding to (111), (220), and (311) lattice planes of diamond. This confirms the diamond nature of the N-DNRs, although Raman spectrum of N-DNRs contains very small Γ_{2g}-band corresponding to sp^3-bonds (see spectrum IV, Fig. S4 of the Supplementary information). There appears a diffused ring in the center of the SAED pattern, indicating the existence of large proportion of sp^2-bonded carbon in this material. A high-resolution ADF-STEM image [Fig. 5(b)] shows that the N-DNRs contain structural defects such as stacking faults and twins.

In Fig. 5(c), a typical selective area EELS spectrum was plotted for the N-DNRs shown in Fig. 5(a). The sp^2 and sp^3 phases were obtained by fitting the experimental spectra to the references of graphite and diamond using the EELS model software.[15] This carbon *K*-edge spectrum exhibits a sharp peak at 289.5 eV (σ* band) and a dip in the vicinity of 302.0 eV representing the typical EELS signal of sp^3-bonded carbon (the diamond). Moreover, there exists a small shoulder or bump at 285.0 eV (π* band) signifying the sp^2-bonded carbon.[16,17] This observation revealed the existence of sp^2 phases not only at the surface, which is observed from x-ray photoelectron spectroscopy studies (XPS; Fig. S5 of the Supplementary information), but also exist in the bulk of the N-DNRs. Figure 5(d) shows the STEM-EELS mapping with sp^3-diamond (*D*, blue color) and sp^2-graphite (*G*, pink color) for the same region depicted in Fig. 5(a), revealing the presence of sp^2 and sp^3 phases simultaneously in the N-DNRs. On the basis of ADF-STEM investigations, it is noticed that the bulk of the N-DNR is a nanohybrid material, which consists of nano-sized diamond grains (sp^3-bonded carbon) along with nanographites (sp^2-bonded carbon) at the grain boundaries and the surface of the nanorods, which is in accord with the findings from Raman and XPS investigations (Figs. S4 and S5 of the Supplementary information).

Consequently, the induction of nanographitic phases formed at the grain boundaries of the N-DNRs is due to the incorporation of N in the N-DF film's growth plasma and the induction of sp^2-bonds at the surface results from the RIE process.

https://doi.org/10.1557/mrc.2018.158

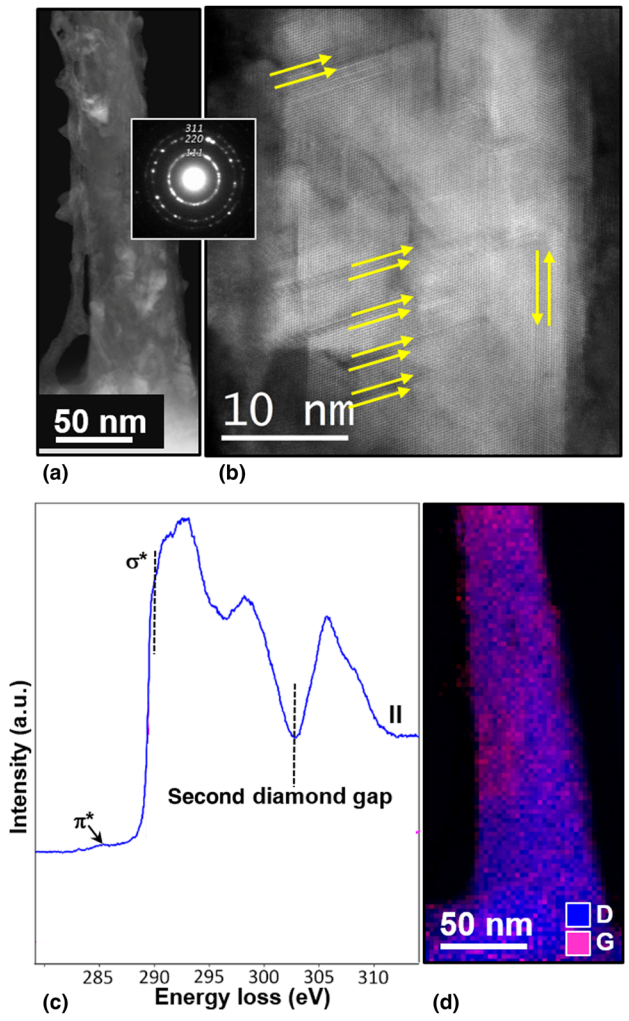

Figure 5. (a) Typical cross-sectional ADF-STEM micrograph of a N-DNR with corresponding SAED shown as inset, (b) high-resolution ADF-STEM image of a N-DNR, (c) EELS core-loss spectrum, and (d) composed EELS elemental mapping for diamond (blue) and graphite (pink) corresponding to Fig. 5(a).

The presence of nanographitic phases leads to lower φ value (4.5 eV) for N-DNRs as compared with U-DNRs. From these observations, we can assume that the interconnected nanographitic phases forming conducting paths in the N-DNRs for transporting electrons to the emitting surface. Once the electrons reach the tip of the N-DNRs with high aspect ratio, they can be emitted into the vacuum without any difficulty as the diamond surfaces show negative electron affinity in nature due to H_2-termination.[18,19] However, the φ value of N-DNRs estimated from Fig. 4(b) [$(\varphi)_{\text{N-DNRs}} = 4.5$ eV] is large as compared with those reported for other diamond materials (Table SII of the Supplementary information). A tailoring of the type of dopants and the doping concentration in N-DFs could result in the decrease in the φ-value, which may further improve the thermionic operation of these nanostructures.

Discussion

The TEE parameters listed in Table I reveal that nanostructuring the DFs markedly changes the Richardson constant of the materials and the extent of modification on this parameter depends on whether the materials are conductive or not. Actually, it is observed for the first time that the Richardson constant of a material can be increased via the change in morphology, mainly the formation of nanorods due to RIE process. The theoretical value for Richardson constant is about 120 A/cm^2 K^2.[20] In practical TEE devices, the Richardson constant of the practical cathode materials is markedly smaller than the theoretical value due to imperfection of the materials, such as low conductivity of the materials, which decreases the effective transport of electrons and insufficient number of sites to emit the electrons efficiently. Paxton et al. observed that the as-prepared N-doped diamond/Mo cathodes emit electrons reasonably well ($J_{\text{TEE}} \sim 22$ nA), following the R–D equation against the temperature, until ~800 °C (with $\varphi = 2.25$ eV and $A_{\text{R}} = 9.97 \times 10^{-4}$ A/cm^2, which were deduced from the J_{TEE}–T curves using R–D model).[21] The current then began to decrease with temperature to maximum test temperature at about 900 °C. Upon reheating, the cathode showed no measureable emission current that is ascribed to the desorption of the H_2 bonded at the surface. The samples regain thermionic emission capacity to $J_{\text{TEE}} = 6$ mA after they were post-treated with hydrogen plasma (with $\varphi = 2.22$ eV and $A_{\text{R}} = 5.96$ A/cm^2). That is, they observed that the hydrogen plasma treatment re-adsorbed the hydrogen on the cathode, which were previously desorbed with hydrogen due to high-temperature operation dramatically increased the Richardson constant for four order of magnitude, and hence markedly increased the TEE current density. This process had little effect on modifying the work function of the N-doped diamond. These observations indicate the importance of forming the sufficient number of electron emission sites on the surface of cathode materials, and the Richardson constant is a measure of the number density of the electron emission sites. Moreover, Kato et al. observed that increasing the phosphorus content in a H-terminated diamond/Mo films improved the TEE capacity of about two orders of magnitude that is mainly owing to the increase in Richardson constant from 10 μA/cm^2 K^2 for lightly P-doped diamond/Mo films for about six orders of magnitude to 15 A/cm^2 K^2 for heavily P-doped films.[22] The work function of the materials was increased from $\varphi = 0.9$ to 2.3 eV due to the increase in phosphorus concentration that contributed much less on increasing the J_{TEE}-value. Moreover, Koeck et al. also observed that in sulfur-doped MCD/Mo films, the Richardson constant changes markedly (2.2–40.0 A/cm^2 K^2), whereas the work function varied insignificantly ($\varphi = 2.3$–2.5 eV) due to the change in sulfur concentration in DFs.[23,24] These observations indicate that the increase in Richardson constant is also an effective approach, besides the decrease in work function, to improve the performance of the TEE cathode materials. It seems that the possible way of enlarging the Richardson

https://doi.org/10.1557/mrc.2018.158

constant of a cathode materials is the increase in emission site density of the cathode materials, or the increase in conductivity of the materials by the increase in donors (phosphorus or sulfur) concentration, as the increase in concentration of donors, which can donate electrons to the cathode materials, is equivalent to the increase in the number density for electron emission sites.

In our studies, incorporation of nitrogen into DFs markedly increased the Richardson constant from $(A_R)_{U\text{-}DF} = 0.05$ mA/cm^2 K^2 for U-DFs to $(A_R)_{N\text{-}DF} = 3.8$ mA/cm^2 K^2 for N-DFs (see Table I) that is close to the improvement in conductivity of DFs, which, in turn, is resulted from the formation of nanographitic phase along the grain boundaries of the diamond materials. The work function was insignificantly altered $(\varphi)_{U\text{-}DF} = 5.0$ eV and $(\varphi)_{N\text{-}DF} = 4.8$ eV (see Table I). Moreover, we observed that the formation of DNRs via RIE process further increases the Richardson constant of N-DFs for about five times [$(A_R)_{N\text{-}DF} = 3.8$ mA/cm^2 K^2 for N-DFs and $(A_R)_{N\text{-}DNRs} = 18.0$ mA/cm^2 K^2 for N-DNRs] without modifying the work function values [$(\varphi)_{N\text{-}DF} = 4.8$ and $(\varphi)_{N\text{-}DNRs} = 4.5$ eV]. The increase in Richardson constant for N-DNRs materials compared with that for N-DFs is presumably owing to the increase in the number density of emission sites, which, in turn, is due to the increase in surface area, which is equivalent to the increase in the proportion of electron emission sites.

On the other hand, the formation of U-DNRs also increases largely the number density of emission sites due to the increase in surface area but is not effective in increasing the Richardson constant of the cathode materials. The possible reason is that the U-DF is resistive that limits the transport of the electrons. The increase in surface area does not enhance the thermionic emission of electrons capacity due to the lack of electron supply to the emission sites. Restated, in order to effectively increase the Richardson constant of a cathode material in a thermionic emission device, nanostructuring the emitting surface is an efficient way, provided that the cathode materials by themselves possess a sufficient electrical conductivity.

Conclusions

As a prospective building block for the next generation of devices, one-dimensional nanostructured materials are promising tools in a vast field of applications. Using ND particle-masked N-DFs as templates, highly ordered vertically aligned N-DNRs were fabricated via O_2-plasma RIE process. For comparison, U-DNRs were fabricated from U-DFs. The characterization studies reveal that the N-DNRs comprise nano-sized diamond grains along with sp^2-graphitic phases at the grain boundaries and the surface of the nanorods, displaying as a nanohybrid material. The thermionic emitter that used N-DNRs as cathode exhibits a high J_{TEE} of 12.0 mA/cm^2, the φ value of 4.5 eV and A_R value of 18.0 A/cm^2 K^2 with an applied voltage of 3 V at 923 K. Moreover, at 773 K the N-DNRs show a life-time stability for a duration of 6000 min at an applied voltage of 3 V. The TEE properties of N-DNRs are superior to those of the U-DNRs, which are attributed to the combined effect of the induction of abundant sp^2-graphitic phases at the grain boundaries and the field penetration effect through the local field enhancement from nanorods owing to a high aspect ratio and an excellent field enhancement factor. The present approach on N-DNRs-based thermionic emitters could considerably reduce power requirements for conventional thermionic electron sources.

Supplementary material

The supplementary material for this article can be found at https://doi.org/10.1557/mrc.2018.158

Acknowledgments

The authors thank the financial support of the Research Foundation Flanders (FWO) via Research Grant 12I8416N and Research Project 1519817N, and the Methusalem "NANO" network. The Hercules Foundation Flanders is acknowledged for financial support of the Raman equipment. The Qu-Ant-EM microscope used for the TEM experiments was partly funded by the Hercules fund from the Flemish Government. S.K. and J.V. acknowledge funding from GOA project "Solarpaint" of the University of Antwerp. K.J. Sankaran and P. Pobedinskas are Postdoctoral Fellows of FWO.

Author contributions

K.J.S., K.H., and I.N. Lin conceived and designed the experiments, synthesized the samples and wrote the manuscript with inputs from all the co-authors. S.D., P.P., and M.K.V.B. performed the SEM and Raman spectroscopy measurements. S.D. and S.S.R. performed the KPFM imaging experiments. S.K., J.V., C.J.Y., and K.C.L. performed the electron microscopic imaging and EEL spectroscopy measurements. J.P.T. and K.T.L. performed the XPS measurements.

Competing financial interests statement

None.

Conflict of interest

None.

References

1. J.W. Schwede, I. Bargatin, D.C. Riley, B.E. Hardin, S.J. Rosenthal, Y. Sun, F. Schmitt, P. Pianetta, R.T. Howe, Z.X. Shen, and N.A. Melosh: Photon-enhanced thermionic emission for solar concentrator systems. *Nat. Mater.* **9**, 762 (2010).
2. I.N. Lin, S. Koizumi, J. Yater, and F. Koeck: Diamond electron emission. *MRS Bull.* **39**, 533 (2014).
3. R. Wanke, W. Voesch, I. Rastegar, A. Kyriazis, W. Braun, and J. Mannhart: Thermoelectronic energy conversion: concepts and materials. *MRS Bull.* **42**, 518 (2017).
4. K.A.A. Khalid, T.J. Leong, and K. Mohamed: Review on thermionic energy converters. *IEEE Trans. Electron Devices* **63**, 2231 (2016).
5. W.A. Kern and D.A. Puotinen: Cleaning solutions based on hydrogen peroxide for use in silicon semiconductor technology. *RCA Rev.* **31**, 187 (1970).

6. O.A. Williams, O. Douheret, M. Daenen, K. Haenen, E. Osawa, and M. Takahashi: Enhanced diamond nucleation on monodispersed nanocrystalline diamond. *Chem. Phys. Lett.* **445**, 255 (2007).
7. S. Tian, Y. Li, X. Xia, C. Gu, and J. Li: Highly efficient field emission from nanodiamond films treated by fast reactive ion etching process. *Physica E* **43**, 1902 (2011).
8. S. Deshmukh, K.J. Sankaran, K. Srinivasu, S. Korneychuk, D. Banerjee, A. Barman, G. Bhattacharya, D.M. Phase, M. Gupta, J. Verbeeck, K. C. Leou, I.N. Lin, K. Haenen, and S.S. Roy: Local probing of the enhanced field electron emission of vertically aligned nitrogen-doped diamond nanorods and their plasma illumination properties. *Diamond Relat. Mater.* **83**, 118 (2018).
9. A. Dato, V. Radmilovic, Z. Lee, J. Philips, and M. Frenklach: Substrate-free gas-phase synthesis of graphene sheets. *Nano Lett.* **8**, 2012 (2008).
10. S. Kunuku, K.J. Sankaran, C.Y. Tsai, W.H. Chang, N.H. Tai, K.C. Leou, and I.N. Lin: Investigations on diamond nanostructuring of different morphologies by the reactive-ion etching process and their potential applications. *ACS Appl. Mater. Interfaces* **5**, 7439 (2013).
11. W.J. Zhang, Y. Wu, C.Y. Cha, W.K. Wong, X.M. Meng, I. Bello, Y. Lifshitz, and S.T. Lee: Structuring single- and nano-crystalline diamond cones. *Diamond Relat. Mater.* **13**, 1037 (2004).
12. N. Yang, U. Hiroshi, O.A. Williams, E. Osawa, N. Tokuda, and C.E. Nebel: Vertically aligned diamond nanowires: fabrication, characterization, and application for DNA sensing. *Phys. Status Solidi A* **206**, 2048 (2009).
13. M. Kataoka, N. Morioka, Y. Kimura, S. Sobue, H. Kato, D. Takeuchi, and S. Yamasaki: Enhanced thermionic electron emission from a stacked structure of phosphorus-doped diamond with a nitrogen-doped diamond surface layer. *Phys. Status Solidi A* **213**, 2650 (2016).
14. F. Jin, Y. Liu, and C.M. Day: Thermionic emission from carbon nanotubes with a thin layer of low work function barium strontium oxide surface coating. *Appl. Phys. Lett.* **88**, 163116 (2006).
15. J. Verbeeck and S. Van Aert: Model based quantification of EELS spectra. *Ultramicroscopy* **101**, 207 (2004).
16. D.M. Gruen, S. Liu, A.R. Krauss, J. Luo, and X. Pan: Fullerenes as precursors for diamond film growth without hydrogen or oxygen additions. *Appl. Phys. Lett.* **64**, 1502 (1994).
17. P. Kovarik, E.B.D. Bourdon, and R.H. Prince: Electron-energy-loss characterization of laser-deposited a-C, a-C:H, and diamond films. *Phys. Rev. B* **48**, 12123 (1993).
18. H. Yamaguchi, T. Masuzawa, S. Nozue, Y. Kudo, I. Saito, J. Koe, M. Kudo, T. Yamada, Y. Takakuwa, and K. Okano: Electron emission from conduction band of diamond with negative electron affinity. *Phys. Rev. B* **80**, 165321 (2009).
19. F.A.M. Koeck, R.J. Nemanich, Y. Balasubramaniam, K. Haenen, and J. Sharp: Enhanced thermionic energy conversion and the thermionic emission from doped diamond films through methane exposure. *Diamond Relat. Mater.* **20**, 1229 (2011).
20. F.A.M. Koeck and R.J. Nemanich: Substrate-diamond interface considerations for enhanced thermionic electron emission from nitrogen doped diamond films. *J. Appl. Phys.* **112**, 113707 (2012).
21. W.F. Paxton, M. Howell, and W.P. Kang: Influence of hydrogen on the thermionic electron emission from nitrogen-incorporated polycrystalline diamond films. *J. Vac. Sci. Technol. B* **30**, 021202 (2012).
22. H. Kato, D. Takeuchi, M. Ogura, T. Yamada, M. Kataoka, Y. Kimura, S. Sobue, C.E. Nebel, and S. Yamasaki: Heavily phosphorus-doped nanocrystalline diamond electrode for thermionic emission application. *Diamond Relat. Mater.* **63**, 165 (2016).
23. F.A.M. Koeck, J.M. Garguilo, and R.J. Nemanich: Field enhanced thermionic electron emission from sulfur doped nanocrystalline diamond films. *Diamond Relat. Mater.* **14**, 704 (2005).
24. F.A.M. Koeck and R.J. Nemanich: Sulfur doped nanocrystalline diamond films as field enhancement based thermionic emitters and their role in energy conversion. *Diamond Relat. Mater.* **14**, 2051 (2005).

https://doi.org/10.1557/mrc.2018.158